

TRAVELLING WAVES AND OSCILLATIONS IN SAL'NIKOV'S COMBUSTION REACTION IN A COMPRESSIBLE GAS

RHYS A. PAUL^{✉1} and LAWRENCE K. FORBES¹

(Received 12 March, 2014; revised 28 October, 2014; first published online 19 January 2015)

Abstract

We consider a two-step Sal'nikov reaction scheme occurring within a compressible viscous gas. The first step of the reaction may be either endothermic or exothermic, while the second step is strictly exothermic. Energy may also be lost from the system due to Newtonian cooling. An asymptotic solution for temperature perturbations of small amplitude is presented using the methods of strained coordinates and multiple scales, and a travelling wave solution with a sech-squared profile is derived. The method of lines is then used to approximate the full system with a set of ordinary differential equations, which are integrated numerically to track accurately the evolution of the reaction front. This numerical method is used to verify the asymptotic solution and investigate behaviours under different conditions. Using this method, temperature waves progressing as pulsatile fronts are detected at appropriate parameter values.

2010 *Mathematics subject classification*: 76N15.

Keywords and phrases: Sal'nikov reaction, combustion, solitons, pulsatile waves, strained coordinates, multiple scales, method of lines.

1. Introduction

In 1949 the Russian scientist Sal'nikov [17] analysed a simple chemical model, which now bears his name. This model considered a mechanism in which a chemical species, A , decays to an inert species, P , by way of an intermediate stage X , with each step occurring at a temperature-sensitive rate. The reaction system may be considered in isolation, such that the only dependent quantities are the chemical concentration and temperature. This seemingly simple scheme can display highly varied behaviour and has been the subject of thorough study. It is well known that such a system may lead to self-sustaining periodic fluctuations in concentration and temperature, the so-called *thermokinetic oscillator*. The conditions necessary for these behaviours have

¹School of Mathematics and Physics, University of Tasmania, Tasmania 7001, Australia;
e-mail: Rhys.Paul@utas.edu.au, Larry.Forbes@utas.edu.au.

© Australian Mathematical Society 2015, Serial-fee code 1446-1811/2015 \$16.00

been studied extensively, and an in-depth investigation by Gray and Roberts [11] has found multiple regions of the parameter space with oscillatory behaviour as well as an unstable orbit surrounding a stable one. These regions have been further investigated by Forbes [6], Forbes et al. [10] and Nelson and Sidhu [16]. These oscillations were observed experimentally by Coppersthaite et al. [4], who noted temperature spikes of more than 200 K in the reaction of hydrogen and chlorine gases.

It is also well known that such a model can have travelling wave solutions, a phenomenon which has roots in the study of reaction diffusion equations made famous by the work of Fisher [5] and Kolmogorov et al. [12]. Barenblatt et al. [2] provided a derivation of differential equations which model chemical reactions such that the reagents are subject to the equations of fluid dynamics. Such a model was considered by Forbes and Derrick [8], who demonstrated the existence of a travelling wave solution with a sech-squared temperature profile. Under the right conditions, this solution evolved a steep shock front resulting in the complete exhaustion of the chemical components behind the reaction front.

In certain circumstances, the system may exhibit both oscillatory and travelling wave behaviour simultaneously, manifesting as travelling waves of nonconstant but periodic amplitude and wave speed. Such solutions have been noted by Weber et al. [20], who used adaptive numerical techniques to model the evolution of combustion waves in gases and solids, and similar results have been observed by Matkowsky and Sivashinsky [14] and Bayliss and Matkowsky [3]; however, the authors assumed the fuel itself to be stationary within the reaction vessel. In this paper, we consider a Sal'nikov reaction scheme in which the reactions occur between compressible viscous gases modelled as a nonstationary fluid governed by the conservation of mass and Navier–Stokes equations. Using the method of multiple scales, we show that the leading order approximation for the behaviour of the gas velocity is a viscous Burgers' equation, in which the viscous term depends on the parameters of the two reaction steps, the bulk viscosity and the diffusion rate of the gas mixture.

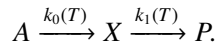
The solutions to Burgers' equation are well documented, owing largely to the Cole–Hopf transform under which it reduces to the heat equation (see Whitham [21, p. 97]). Of particular interest in this paper are the travelling wave solutions, which manifest as a sech-squared temperature profile, and pulsatile solutions, in which the wave front propagates with periodic amplitude and wave speed. When the viscosity term is small, Burgers' equation is capable of developing steep fronts, which become shocks in the inviscid limit. When two of these shocks interact, they are known to merge, forming a larger shock whose speed is between the speeds of the initial profiles. All of these behaviours are described by Whitham [21, pp. 96–112].

In Section 2, we present the model and its governing equations. In Section 3, we present a weakly nonlinear approximation of the system using asymptotic expansions based on the methods of strained coordinates and multiple time scales, and a travelling wave solution to this approximation is then considered in Section 4. A numerical scheme is derived in Section 5 to solve the full nonlinear problem, and it confirms the travelling waves predicted by the weakly nonlinear theory. In addition, pulsatile wave

fronts are obtained and a sample solution is presented. The paper concludes with a discussion in Section 6.

2. Combustion model

Consider a pipe of infinite length positioned such that it extends along the x -axis. Inside the pipe a chemical species, A , decays to an intermediate species, X , at a rate, k_0 , which is dependent on temperature, T . This decay may proceed endothermically or exothermically. The species, X , then decays exothermically to a chemically inert species, P , at a temperature-dependent rate, k_1 . Schematically, we represent this reaction process as follows:



The gas flow is assumed to be one dimensional and the only spatial variation in the gas properties is in the direction of the x -axis. It is also assumed that the concentration of species, A , is in such an excess that it remains effectively constant as the reactions proceed; the assumption $[A] = \text{constant}$ is known as the *pool-chemical approximation* (see for example Scott [18, p. 31]). The gas density, ρ , is governed by the convection–diffusion equation, which, assuming Fick’s laws of diffusion and constant diffusion coefficient, S , is given by

$$\frac{\partial \rho}{\partial t} + \frac{\partial}{\partial x}(\rho u) = S \frac{\partial^2 \rho}{\partial x^2}, \quad (2.1)$$

in which u is the gas speed along the x -axis. A simple derivation of equation (2.1) is given by Stocker [19, p. 56]. It follows from a similar argument that the concentration of species X , denoted $[X]$, satisfies the equation

$$\frac{\partial [X]}{\partial t} + \frac{\partial}{\partial x}(u[X]) = [A]k_0(T) - [X]k_1(T) + S \frac{\partial^2 [X]}{\partial x^2}, \quad (2.2)$$

wherein $[A]$ is the molar concentration of A . Denoting the pressure of the gas as p and its bulk viscosity as ν , the Navier–Stokes equation for viscous and compressible fluids may be written as

$$\frac{\partial}{\partial t}(\rho u) + \frac{\partial}{\partial x}(\rho u^2 + p) = \frac{4}{3}\nu \frac{\partial^2 u}{\partial x^2}. \quad (2.3)$$

We may also relate the pressure of the gas to its density and temperature using the ideal gas law

$$p = \rho RT, \quad (2.4)$$

in which R is the universal gas constant. Finally, we consider the balancing of energy in the system. Defining γ to be the ratio of specific heats of the gas, B the rate of heat loss due to Newtonian cooling, w the rate of thermal diffusion, Q_0 and Q_1 the enthalpies of creation of X and P , respectively, and T_a the ambient temperature outside the pipe, the energy equation is

$$\begin{aligned} & \frac{\partial}{\partial t} \left[\rho \left(\frac{\gamma RT}{\gamma - 1} + \frac{1}{2} u^2 \right) \right] + \frac{\partial}{\partial x} \left[u \rho \left(\frac{\gamma RT}{\gamma - 1} + \frac{1}{2} u^2 \right) \right] - \frac{\partial p}{\partial t} \\ & = w \frac{\partial^2 T}{\partial x^2} + \frac{4}{3} \nu \frac{\partial}{\partial x} \left(u \frac{\partial u}{\partial x} \right) + Q_0 [A] k_0(T) + Q_1 [X] k_1(T) - B(T - T_a). \end{aligned} \quad (2.5)$$

Equations (2.3) and (2.5) follow from the derivations given by Liepmann and Roshko [13, p. 337] with a little algebra. Far ahead of the reaction front, we expect the system to attain its unperturbed state, and so we introduce the upstream boundary conditions

$$p \rightarrow \rho_0 RT_a, \quad \rho \rightarrow \rho_0, \quad u \rightarrow 0, \quad T \rightarrow T_a, \quad [X] \rightarrow [X]_0 \quad \text{as } x \rightarrow \infty.$$

Before nondimensionalising, we must consider the forms of the reaction rates $k_0(T)$ and $k_1(T)$. Assuming Arrhenius reaction kinetics (see Williams [22, p. 373]), these rates are

$$k_0(T) = z_0 e^{-E_0/RT}, \\ k_1(T) = z_1 e^{-E_1/RT},$$

where E_0 and E_1 are the activation energies of the respective reactions and z_0 and z_1 are the reaction coefficients. Although alternative forms for these rates may be chosen later, we will nevertheless make use of their activation energies and reaction coefficients to define dimensionless parameters. We now proceed to introduce nondimensional variables in relation to appropriate scales. The reference length is chosen to be $\sqrt{E_1}/z_1$, the time scale is $1/z_1$ and, consequently, the speed scale is $\sqrt{E_1}$. Temperature is scaled relative to the quantity E_1/R and the upstream density ρ_0 provides the reference for the density. This then suggests the quantity $\rho_0 E_1$ as the natural choice to scale pressure. Finally, we scale concentration relative to the quantity $\rho_0 E_1/Q_1$. We now introduce nine new dimensionless parameters

$$\mu = \frac{4z_1\nu}{3\rho_0 E_1}, \quad \beta = \frac{B}{z_1\rho_0 R}, \quad \phi = \frac{z_1 w}{\rho_0 E_1 R}, \quad \zeta = \frac{z_0}{z_1}, \\ q = \frac{Q_0}{Q_1}, \quad \epsilon = \frac{E_0}{E_1}, \quad \sigma = \frac{z_1 S}{E_1}, \quad \theta_a = \frac{RT_a}{E_1}, \quad A = \frac{[A]Q_1}{\rho_0 E_1},$$

where the constant μ represents the dimensionless bulk viscosity, β the rate of Newtonian cooling, ϕ the rate of thermal diffusion, σ the rate of diffusion of both X and ρ , A the dimensionless concentration of chemical A and θ_a the ambient temperature. The quantities ζ , q and ϵ represent the ratio of reaction coefficients, heat of reaction and activation energies of each of the reaction steps, respectively.

From here onwards, we will drop the square bracket notation used to denote concentration and molar concentration. As such, the transport equation (2.2) becomes

$$\frac{\partial X}{\partial t} + \frac{\partial}{\partial x}(uX) = \zeta A k_0(T) - X k_1(T) + \sigma \frac{\partial^2 X}{\partial x^2}, \quad (2.6)$$

where the Arrhenius reaction rates k_0 and k_1 are now

$$k_0(T) = e^{-\epsilon/T}, \\ k_1(T) = e^{-1/T}. \quad (2.7)$$

The conservation of mass equation (2.1) becomes

$$\frac{\partial \rho}{\partial t} + \frac{\partial}{\partial x}(\rho u) = \sigma \frac{\partial^2 \rho}{\partial x^2}, \quad (2.8)$$

while the momentum equation (2.3) yields

$$\frac{\partial}{\partial t}(\rho u) + \frac{\partial}{\partial x}(\rho u^2 + p) = \mu \frac{\partial^2 u}{\partial x^2}. \tag{2.9}$$

The energy equation (2.5) is

$$\begin{aligned} & \frac{\partial}{\partial t} \left[\rho \left(\frac{\gamma T}{\gamma - 1} + \frac{1}{2} u^2 \right) \right] + \frac{\partial}{\partial x} \left[u \rho \left(\frac{\gamma T}{\gamma - 1} + \frac{1}{2} u^2 \right) \right] \\ & = \frac{\partial p}{\partial t} + \phi \frac{\partial^2 T}{\partial x^2} + \mu \frac{\partial}{\partial x} \left(u \frac{\partial u}{\partial x} \right) + q\zeta A k_0(T) + X k_1(T) - \beta(T - T_a), \end{aligned} \tag{2.10}$$

and the gas law (2.4) has the form

$$p = \rho T. \tag{2.11}$$

Finally, the upstream boundary conditions become

$$p \rightarrow \theta_a, \quad \rho \rightarrow 1, \quad u \rightarrow 0, \quad T \rightarrow \theta_a, \quad X \rightarrow X_0 \quad \text{as } x \rightarrow \infty.$$

3. Weakly nonlinear analysis

In this section, we use the method of strained coordinates with the method of multiple scales to derive a set of equations which approximate the behaviour of the model outlined in Section 2 for small-amplitude perturbations. We do so by assuming that the values vary from their steady-state solutions by a small value, characterised by the parameter κ . Much of this analysis is similar to the process used by Forbes [7] and, interestingly, the solutions are qualitatively similar, despite the addition of diffusion and viscosity into the model. Much of the notation in this analysis will be retained for ease of comparison. First we introduce two strained coordinates given by

$$\tilde{t}_1 = \kappa t, \quad \tilde{x} = \kappa x.$$

We also introduce a second time scale, \tilde{t}_2 , defined as

$$\tilde{t}_2 = \kappa^2 t.$$

The dependent variables are now expanded as power series in the small parameter, κ , around their steady states as follows:

$$\begin{aligned} u &= \kappa u_1 + \kappa^2 u_2 + O(\kappa^3), \\ \rho &= 1 + \kappa \rho_1 + \kappa^2 \rho_2 + O(\kappa^3), \\ T &= \theta_a + \kappa T_1 + \kappa^2 T_2 + O(\kappa^3), \\ p &= \theta_a + \kappa p_1 + \kappa^2 p_2 + O(\kappa^3), \\ X &= X_0 + \kappa X_1 + \kappa^2 X_2 + O(\kappa^3). \end{aligned}$$

The Arrhenius reaction rates in (2.7) are now approximated with the two rates

$$\begin{aligned} k_0(T) &= \begin{cases} 0 & \text{if } T \leq \theta_a, \\ 1 - e^{-\epsilon(T-\theta_a)} & \text{if } T > \theta_a, \end{cases} \\ k_1(T) &= \begin{cases} 0 & \text{if } T \leq \theta_a, \\ 1 - e^{-(T-\theta_a)} & \text{if } T > \theta_a. \end{cases} \end{aligned} \tag{3.1}$$

Forms similar to these were used by Forbes and Derrick [8] and Forbes [7], and have the advantage of approximating the qualitative behaviour of the Arrhenius rates (2.7) for large temperatures while avoiding the *cold boundary problem*, in which the reactions proceed for any arbitrarily small positive temperature (see Williams [22, p. 21]). We may now expand these rates in powers of the parameter κ , yielding

$$\begin{aligned} k_0(T) &= \kappa \epsilon T_1 + \kappa^2 (\epsilon T_2 - \frac{1}{2} \epsilon^2 T_1^2) + \mathcal{O}(\kappa^3), \\ k_1(T) &= \kappa T_1 + \kappa^2 (T_2 - \frac{1}{2} T_1^2) + \mathcal{O}(\kappa^3) \end{aligned} \quad (3.2)$$

for $T > \theta_a$. These expansions are substituted into the dimensionless governing equations and coefficients of each power of κ are equated. The order, κ , equation obtained from expanding the energy equation yields

$$T_1(\tilde{x}, \tilde{t}_1, \tilde{t}_2) \equiv 0,$$

which, upon expanding the gas law (2.11), gives the relations

$$p_1 = \theta_a \rho_1, \quad p_2 = T_2 + \theta_a \rho_2$$

at first and second orders in κ . The second-order temperature equation, coupled with the first-order mass equation and the new reaction rate expansion (3.2), yields the equation

$$T_2(\tilde{x}, \tilde{t}_1, \tilde{t}_2) = -\omega \frac{\partial u_1}{\partial \tilde{x}}, \quad (3.3)$$

in which we have defined the constant

$$\omega = \frac{\theta_a}{\beta - \zeta q \epsilon A - X_0}. \quad (3.4)$$

The resulting first-order momentum and mass equations may be cross differentiated to yield

$$\frac{\partial^2 u_1}{\partial \tilde{t}_1^2} = \theta_a \frac{\partial^2 u_1}{\partial \tilde{x}^2}. \quad (3.5)$$

Thus, the fluid speed at first-order obeys a linear wave equation with characteristic speed, $\sqrt{\theta_a}$, on the short time scale. Ahead of further analysis, we define the following constant in terms of ω , in equation (3.4):

$$\Gamma = \frac{1}{\mu + \sigma + \omega}.$$

Then, after some algebraic manipulation of the second-order momentum and mass equations, it can be shown that the variable, u_1 , satisfies the partial differential equation

$$\frac{1}{\Gamma} \frac{\partial^2 u_1}{\partial \tilde{x}^2} - \frac{\partial}{\partial \tilde{x}} (u_1^2) - 2 \frac{\partial u_1}{\partial \tilde{t}_2} = 0 \quad (3.6)$$

in the long time scale, which is of utmost interest here.

4. Travelling waves

A travelling wave solution is sought in terms of the variable

$$\eta = \tilde{x} - \sqrt{\theta_a} \tilde{t}_1 - m \tilde{t}_2. \quad (4.1)$$

This transformation satisfies equation (3.5) identically and, so, that equation is considered no further. Equation (3.6) may now be integrated exactly, yielding

$$\frac{du_1}{d\eta} = \Gamma(u_1 - 2m)u_1, \quad (4.2)$$

which has solution

$$u_1(\eta) = \frac{2m}{1 + \exp(2m\Gamma\eta)}. \quad (4.3)$$

Equation (3.3) now takes the form

$$T_2(\eta) = -\omega \frac{du_1}{d\eta}.$$

Evaluating this expression using equation (4.3) yields

$$T_2(\eta) = m^2 \omega \Gamma \operatorname{sech}^2(m\Gamma\eta), \quad (4.4)$$

and thus the asymptotic representation for temperature is

$$T(x, t) = \theta_a + \kappa^2 m^2 \omega \Gamma \operatorname{sech}^2(\kappa m \Gamma (x - ct)) + O(\kappa^3).$$

Here c is the wave speed in the physical coordinates, x and t , and it follows from (4.1) that along a characteristic of (3.5),

$$c = \frac{dx}{dt} = \sqrt{\theta_a} + \kappa m + O(\kappa^2). \quad (4.5)$$

We may now make use of the first-order mass equation and second-order transport equation to find the forms of the density and concentration profiles. The resulting expressions are

$$\rho_1(\eta) = \frac{2m}{\sqrt{\theta_a} [1 + \exp(2m\Gamma\eta)]}$$

and

$$X_1(\eta) = \frac{2m(X_0 - X_0\omega + \omega\zeta\epsilon A)}{\sqrt{\theta_a} [1 + \exp(2m\Gamma\eta)]}.$$

Notice that the amplitude of the solution (4.4) could in fact be negative, corresponding to a *cold soliton* if $\omega\Gamma < 0$. However, in the present model, this is precluded by the assumption, $T > \theta_a$, in equation (3.2). Nevertheless, *cold soliton* solutions might be possible for more complex reaction systems, in which the full Arrhenius reaction rates are included.

5. Numerical analysis

We now proceed to analyse the full system of partial differential equations (2.6) and (2.8)–(2.11) by approximating them with a set of ordinary differential equations using the method of lines (see Ames [1, p. 193]). We do so by approximating the infinite pipe with one of length $2L$, discretising the spatial coordinate $-L \leq x \leq L$ into N mesh points and replacing the corresponding spatial derivatives with appropriate centred finite differences. Using a j subscript to represent the value of a dependent variable at the j th spatial mesh point, a prime to represent temporal derivatives and letting Δx be the width between mesh points, the governing equations may be approximated by

$$\rho'_j = \frac{\rho_j(u_{j-1} - u_{j+1}) + u_j(\rho_{j-1} - \rho_{j+1})}{2\Delta x} + \sigma \left(\frac{\rho_{j+1} - 2\rho_j + \rho_{j-1}}{\Delta x^2} \right), \tag{5.1}$$

$$u'_j = \frac{2u_j(u_{j-1} - u_{j+1}) + T_{j-1} - T_{j+1}}{2\Delta x} + \frac{1}{\rho_j} \left[\frac{(T_j + u_j^2)(\rho_{j-1} - \rho_{j+1})}{2\Delta x} - u_j \rho'_j + \mu \left(\frac{u_{j+1} - 2u_j + u_{j-1}}{\Delta x^2} \right) \right], \tag{5.2}$$

$$T'_j = (\gamma - 1) \left\{ u_j \left(\frac{J_{j-1} - J_{j+1}}{2\Delta x} - u'_j \right) + \frac{J_j(u_{j-1} - u_{j+1})}{2\Delta x} + \frac{1}{\rho_j} \left[\mu \left(\frac{u_j(u_{j+1} - 2u_j + u_{j-1})}{\Delta x^2} + \left(\frac{u_{j+1} - u_{j-1}}{2\Delta x} \right)^2 \right) + \frac{J_j u_j (\rho_{j-1} - \rho_{j+1})}{2\Delta x} + \phi \left(\frac{T_{j+1} - 2T_j + T_{j-1}}{\Delta x^2} \right) + \rho'_j (T_j - J_j) + X_j k_0(T_j) + \zeta q A k_1(T_j) - \beta(T_j - \theta_a) \right] \right\}, \tag{5.3}$$

$$X'_j = \zeta A k_0(T_j) - X_j k_1(T_j) + \frac{X_j(u_{j-1} - u_{j+1}) + u_j(X_{j-1} - X_{j+1})}{2\Delta x} + \sigma \left(\frac{X_{j+1} - 2X_j + X_{j-1}}{\Delta x^2} \right) \tag{5.4}$$

for $1 \leq j \leq N$. In equation (5.3), we have defined the quantity

$$J_j = \frac{\gamma T_j}{\gamma - 1} + \frac{1}{2} u_j^2,$$

the total enthalpy of the gas (see Liepmann and Roshko [13, p. 190]) at the j th mesh point, for convenience. The reaction rates may be used in their approximated form (3.1), evaluated at the mesh point x_j . The best choice of boundary conditions is not obvious, since the only conditions on the original system were those which applied far upstream. For this analysis, we have chosen to enforce zero-derivative conditions for each dependent variable at both ends of the mesh. This is achieved by introducing *false boundaries* at $x = -(L + \Delta x)$ and $x = L + \Delta x$, which correspond to mesh points at $j = 0$ and $j = N + 1$, respectively. Approximating the derivatives with appropriate central finite differences, these conditions on the gas speed u reduce to

$$u_0 = u_2, \quad u_{N+1} = u_{N-1}$$

with similar results holding for ρ , X and T . Further details of this technique are discussed in the book by Ames [1]. This system (5.1)–(5.4) of 5N equations can now be integrated forwards in time using an appropriate method. For this analysis we have used the ode45 routine in MATLAB [15], which uses fourth- and fifth-order Runge–Kutta methods and an adaptive time step to control the error. The starting values are chosen such that the initial temperature has the form

$$T(x, 0) = \theta_a + A_T \operatorname{sech}^2(\kappa m \Gamma(x + x_0)),$$

where A_T is the amplitude of the initial temperature profile and x_0 is an offset for the location of the pulse. The value of x_0 is chosen to position the centre of the initial impulse away from the boundaries, minimising the effects of boundary conditions. The starting values of u , ρ and X are all chosen such that they satisfy the weakly nonlinear system derived in Section 3. As such, they become

$$\begin{aligned} u(x, 0) &= \frac{2\kappa m}{1 + \exp\{2\kappa m \Gamma(x + x_0)\}}, \\ \rho(x, 0) &= 1 + \frac{2\kappa m}{\sqrt{\theta_a}[1 + \exp\{2\kappa m \Gamma(x + x_0)\}]}, \\ X(x, 0) &= X_0 + \frac{2\kappa m(X_0 - X_0\omega + \omega\zeta\epsilon A)}{\sqrt{\theta_a}[1 + \exp\{2\kappa m \Gamma(x + x_0)\}]}. \end{aligned}$$

The parameter combination κm may be calculated using the relation

$$\kappa m = \sqrt{\frac{A_T}{\omega\Gamma}}.$$

Figure 1 displays the temperature above ambient as returned by the numerical solution obtained for parameters $\theta_a = 0.15$, $X_0 = 0.25$, $A = 1$, $\zeta = 0.4$, $q = 0.2$, $\epsilon = 0.75$, $\beta = 1$, $\sigma = 0.1$, $\mu = 0.03$, $\phi = 0.2$ and $\gamma = 1.4$ for times $t = 0, 20, 40, \dots, 500$. The grid spacing is $\Delta x = 0.02$, since this has been found sufficient for the convergence of the numerical results. The initial condition is given perturbation amplitude $A_T = 10^{-4}$ and initial displacement $x_0 = 100$ to the left of the origin. The solution increases slightly in amplitude at first, but continues travelling at a constant speed while maintaining a profile closely matching its initial shape. Analysis of the solution indicates an average wave speed of about 0.397. This value is calculated by simply taking the change in position of the maximum temperature divided by the final time of the numerical scheme (in this case 500). This measured value for the average wave speed is in close agreement with the predicted speed of $\sqrt{\theta_a} + \kappa m \approx 0.400$ in equation (4.5). Figure 2 shows a comparison of the numerical solution (plotted with a solid blue line) with the asymptotic solution (dashed red line) for the same parameters as Figure 1 for times $t = 0, 200, 400, \dots, 1000$. It can be seen that the two solutions are almost identical, and there is little noticeable separation of the two until $t = 1000$. This confirms the usefulness of the weakly nonlinear solution (4.4) in Section 4.

Forbes [7] showed that in the weakly nonlinear case, two sech-squared pulses with different amplitudes could run into each other and form a single larger pulse.

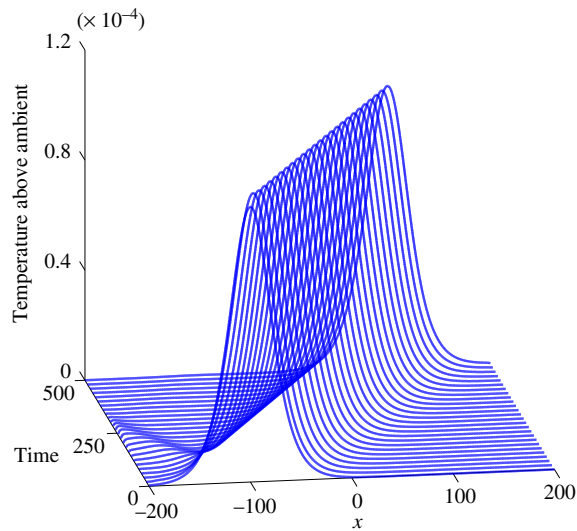


FIGURE 1. Travelling wave solution obtained by the numerical scheme, with parameter values given in the text.

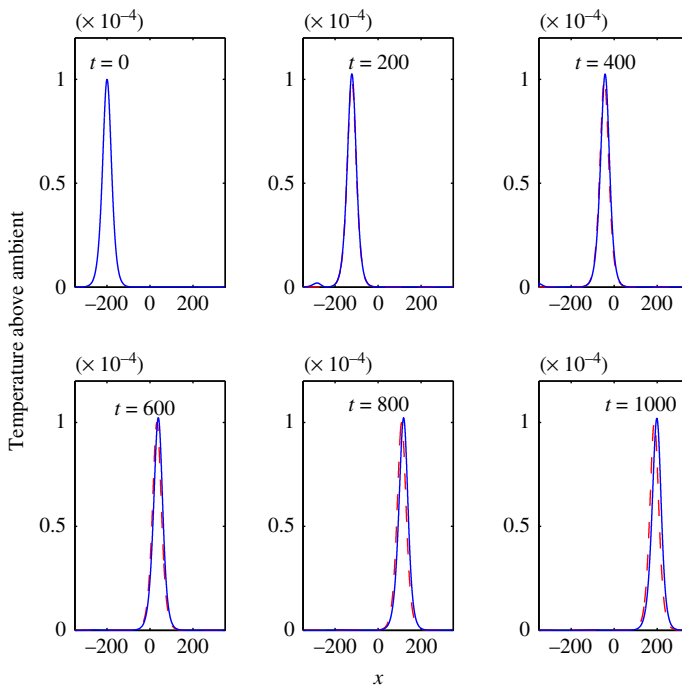


FIGURE 2. Comparison of numerical solution (solid blue line) to asymptotic solution (dashed red line) for the same parameter values illustrated in Figure 1. (Colour available online.)

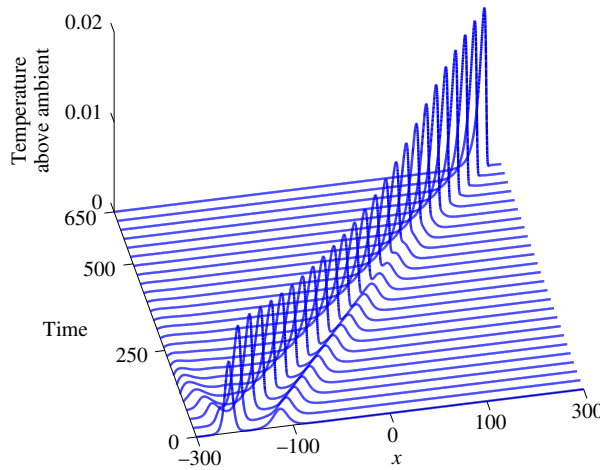


FIGURE 3. Evolution of two sech-squared pulses of differing amplitudes for the parameter values listed in the text.

To investigate whether this is also true for large-amplitude disturbances in the full system, Figure 3 displays the numerical solution to the full system of partial differential equations, given a two-sech-squared pulse starting condition of the form

$$T(x, 0) = \theta_a + A_{T1} \operatorname{sech}^2(\kappa m_1 \Gamma(x + x_{01})) + A_{T2} \operatorname{sech}^2(\kappa m_2 \Gamma(x + x_{02})),$$

where

$$\kappa m_1 = \sqrt{\frac{A_{T1}}{\omega \Gamma}}, \quad \kappa m_2 = \sqrt{\frac{A_{T2}}{\omega \Gamma}}.$$

Here the system parameters are chosen to be $\theta_a = 0.35$, $X_0 = 0.25$, $A = 1$, $\zeta = 0.4$, $q = 0.2$, $\epsilon = 0.75$, $\beta = 1$, $\sigma = 0.25$, $\mu = 0.1$, $\phi = 0.4$ and $\gamma = 1.4$ with initial amplitudes $A_{T1} = 8 \times 10^{-3}$ and $A_{T2} = 2 \times 10^{-3}$. The solution is calculated using spacing $\Delta x = 0.02$ and is displayed at times $t = 0, 26, 52, \dots, 650$. The figure shows that the larger, left-most pulse travels faster than the smaller, right-most pulse and the two eventually meet at around $t = 400$. After coinciding, the two merge to form a single, larger pulse, which continues travelling to the right.

Figure 4 displays the approximate speed of the larger pulse in Figure 3. The wave speed at the point x_j , denoted v_j , was calculated by tracking the position of the maximum temperature in Figure 3 at intervals of one time unit and numerically differentiating the results with a forward finite difference. The numerical differentiation produced rapid, low-amplitude oscillations over several numerical mesh points. In order to reduce these variations, triangular smoothing was employed. The velocity at the position x_j , denoted v_j , was replaced with a weighted average of the nearby values, v_j^* , according to the rule

$$v_j^* = \frac{v_{j-2} + 3v_{j-1} + 5v_j + 3v_{j+1} + v_{j+2}}{13}. \tag{5.5}$$

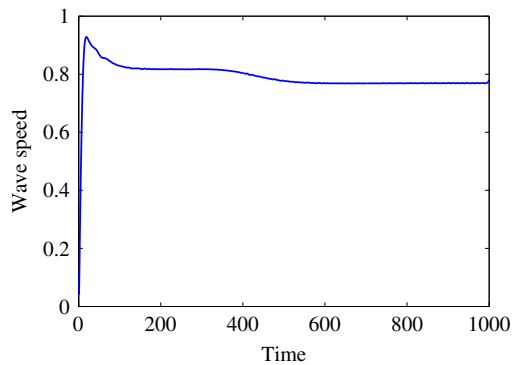


FIGURE 4. Approximate speed of the left-most pulse before and after it interacts with the smaller pulse displayed in Figure 3.

Ten iterations of this procedure were needed before the majority of the variations were smoothed away. From Figure 4, we can see that the speed increases rapidly before settling at a value of around 0.817. Some remaining small-amplitude oscillations may still be visible in this diagram. When the two waves interact the wave speed decreases to about 0.769; behaviour consistent with that of confluent shocks in Burgers' equation (see Whitham [21]). While the equation for the gas speed given in (4.3) is not strictly a shock, it begins to look more like one as $m\Gamma$ becomes large. As such, it is perhaps not too surprising that their behaviours are qualitatively similar.

In the interest of exploration, we have run this system for a different set of parameters but made use of the Arrhenius reaction rates as in (2.7). Figure 5 shows the solution under this scheme with parameter values $\theta_a = 0.15$, $X_0 = 0.4$, $A = 0.8$, $\zeta = 0.3$, $q = 0.1$, $\epsilon = 0.1$, $\beta = 1$, $\sigma = 0.3$, $\mu = 0.2$, $\phi = 0.5$, $\gamma = 1.4$, initial amplitude $A_T = 10^{-2}$ and offset $x_0 = 100$. The solution is displayed for $t = 0, 5, 10, \dots, 350$ and has been calculated with a grid spacing $\Delta x = 0.02$. The temperature quickly increases in amplitude around $t = 60$ and reaches a temperature of $T \approx 2.15$. At this point the wave front (the location of the temperature peak) diverges, forming both forward and backward travelling waves with periodically varying amplitudes and wave speeds. This behaviour continues with more pulsatile wave fronts branching off in both the positive and negative x -directions. Coinciding with each temperature spike, there are large increases in the reaction temperature along the upper and lower lengths of the pipe, independent of the behaviour of the reaction front. These oscillations are caused by the behaviour of the well-mixed reaction system, in which $u \equiv 0$ and there is no spatial variation. They are thus limit cycles in the purely temporal system, and come about through a Hopf bifurcation in the Sal'nikov reaction; further details are given by Forbes and Gray [9]. This behaviour did not occur if the Arrhenius rates were replaced with the approximate rates in (3.1).

The periodic behaviour in the amplitude and wave speed is best illustrated by the right-most wave front. Figure 6 displays the amplitude of this front over time and its

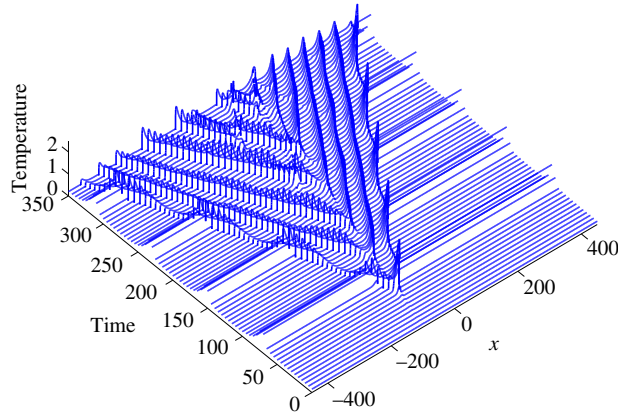


FIGURE 5. Pulsatile travelling wave solution with Arrhenius rates for parameters given in the text. The diagram shows periodic oscillations in time at all positions x , corresponding to the well-mixed system. In addition, a pulsatile travelling wave system moving in each direction is also present.

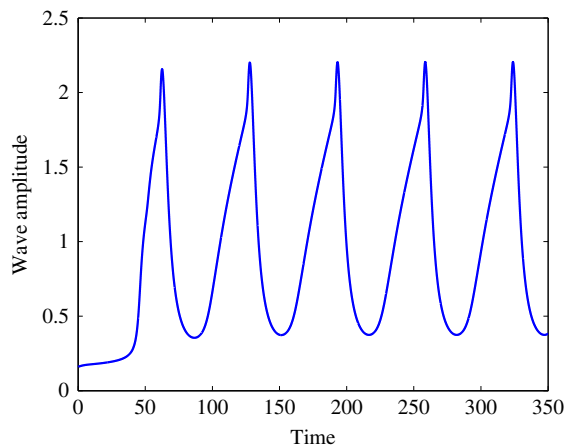


FIGURE 6. Amplitude of right-most wave front of pulsatile solution displayed in Figure 5.

periodic nature is evident. Similar behaviour is observed in the wave speed shown in Figure 7. This plot was produced in much the same way as Figure 4, that is, numerically differentiating the wave position and using one iteration of the smoothing scheme in (5.5) to reduce the rapid variations (some residual oscillations from the numerical differentiation may still be visible at early times). At around $t = 40$ the speed begins to increase rapidly and reaches a value of about 3.3 before decreasing to less than 1. These rapid increases and decreases in wave speed occur approximately every 65 time units, and direct comparison with Figure 6 indicates that wave speed and amplitude maxima coincide. These plots were produced by finding the position

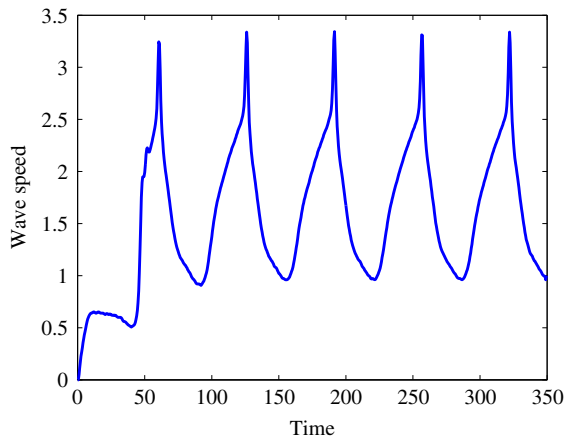


FIGURE 7. Approximate wave speed of the forward front in Figure 5.

and amplitude of the maximum temperature in the domain $[-L, L]$ at the initial time. At the next time step, this domain is updated to $[x_m, L]$, where x_m is the position of the maximum temperature at the previous step, and this process is repeated. This has the effect of tracking the right-most reaction front.

6. Conclusion

We have demonstrated a weakly nonlinear analysis of a Sal'nikov reaction scheme in a viscous and diffusive compressible gas mixture using the methods of strained coordinates and multiple scales. Interestingly, it was demonstrated that the solution to the weakly nonlinear equations governing the system is a sech-squared travelling wave, qualitatively similar to that which was investigated by Forbes [7], despite the inclusion of strong fluid viscosity and diffusion. It is possible to demonstrate the stability of these solutions by considering the behaviour of a perturbation of the form $u_1(\eta) + \hat{u}_1(\eta)$ in equation (4.2). This analysis is identical to the one provided by Forbes in the aforementioned paper and has been excluded in the interest of space. We have also made use of the method of lines to develop a numerical scheme to approximate accurately the behaviour of the full set of governing partial differential equations. Using this scheme, we have numerically verified the conclusion of the weakly nonlinear solution, demonstrating stable travelling wave solutions. In addition, the fully nonlinear system permits pulsatile travelling wave solutions, in which periodic oscillations in the well-mixed system are also present, and such a case has been illustrated.

References

- [1] W. F. Ames, *Numerical methods for partial differential equations* (Academic, New York, 1977).
- [2] G. Barenblatt, Ya. B. Zeldovich, V. B. Librovich and G. Makhviladze, *The mathematical theory of combustion and explosions* (Consultants Bureau, New York, 1985).

- [3] A. Bayliss and B. J. Matkowsky, "Fronts, relaxation oscillations, and period doubling in solid fuel combustion", *J. Comput. Phys.* **71** (1987) 147–168; doi:10.1016/0021-9991(87)90024-6.
- [4] D. P. Coppersthaite, J. F. Griffiths and B. F. Gray, "Oscillations in the hydrogen + chlorine reaction: experimental measurements and numerical simulation", *J. Phys. Chem.* **7** (1991) 6961–6967; doi:10.1021/j100171a043.
- [5] R. A. Fisher, "The wave of advance of advantageous genes", *Ann. Eugen.* **7** (1937) 1–26; doi:10.1111/j.1469-1809.1937.tb02153.x.
- [6] L. K. Forbes, "Limit-cycle behaviour in a model chemical reaction: the Sal'nikov thermokinetic oscillator", *Proc. R. Soc. Lond. Ser. A Math. Phys. Sci.* **430** (1990) 641–651; doi:10.1098/rspa.1990.0110.
- [7] L. K. Forbes, "Thermal solitons: travelling waves in combustion", *Proc. R. Soc. Lond. Ser. A Math. Phys. Eng. Sci.* **469** (2013) 20120587; doi:10.1098/rspa.2012.0587.
- [8] L. K. Forbes and W. Derrick, "A combustion wave of permanent form in a compressible gas", *ANZIAM J.* **43** (2001) 35–58; doi:10.1017/S144618110001141X.
- [9] L. K. Forbes and B. F. Gray, "Forced oscillations in an exothermic chemical reaction", *Dyn. Stab. Syst.* **9** (1994) 253–269; doi:10.1080/0268119408806181.
- [10] L. K. Forbes, M. R. Myerscough and B. F. Gray, "On the presence of limit-cycles in a model exothermic chemical reaction: Sal'nikov's oscillator with two temperature-dependent reaction rates", *Proc. Math. Phys. Sci.* **435** (1991) 591–604; doi:10.2307/52094.
- [11] B. F. Gray and M. J. Roberts, "Analysis of chemical kinetic systems over the entire parameter space I. The Sal'nikov thermokinetic oscillator", *Proc. R. Soc. Lond. Ser. A Math. Phys. Sci.* **416** (1988) 391–402; doi:10.1098/rspa.1988.0040.
- [12] A. N. Kolmogorov, I. G. Petrovskii and N. S. Piskunov, "A study of the equation of diffusion with increase in the quantity of matter, and its application to a biological problem", *Byul. Moskovskogo Gos. Univ.* **1** (1937) 1–26; <http://books.google.com/books?id=ikN59GkYJKIC&lpg=PP1&dq=A.N.Kolmogorov3ASelectedWorks&client=firefox-a&pg=PA242#v=onepage&q=&f=false>.
- [13] H. W. Liepmann and A. Roshko, *Elements of gasdynamics* (Wiley, New York, 1957).
- [14] B. J. Matkowsky and G. I. Sivashinsky, "Propagation of a pulsating reaction front in solid fuel combustion", *SIAM J. Appl. Math.* **35** (1978) 465–478; doi:10.2307/2100631.
- [15] *MATLAB version 8.0.0.783 (R2012b)* (The MathWorks Inc., Natick, USA, 2012).
- [16] M. I. Nelson and H. S. Sidhu, "Bifurcation phenomena for an oxidation reaction in a continuously stirred tank reactor I. Adiabatic operation", *J. Math. Chem.* **31** (2002) 155–186; doi:10.1021/j100171a043.
- [17] I. Ye. Sal'nikov, "Contribution to the theory of the periodic homogeneous chemical reactions", *Zh. Fiz. Khim.* **23** (1949) 258–272.
- [18] S. K. Scott, *Chemical chaos* (Oxford University Press, London, 1993).
- [19] T. Stocker, *Introduction to climate modelling* (Springer, Dordrecht, 2011).
- [20] R. O. Weber, G. N. Mercer, H. S. Sidhu and B. F. Gray, "Combustion waves for gases ($Le = 1$) and solids ($Le \rightarrow \infty$)", *SIAM J. Appl. Math.* **453** (1997) 1105–1118; doi:10.1098/rspa.1997.0062.
- [21] G. B. Whitham, *Linear and nonlinear waves* (Wiley-Interscience, New York, 1993).
- [22] F. A. Williams, *Combustion theory: the fundamental theory of chemically reacting flow systems* (Addison-Wesley, Reading, MA, 1965).